TABLE 2 Comparisons Between the Proposed Antenna and Existing Antennas

Antennas	BW GHz (−10 dB)	Dimension (mm²)	Electrical Dimension	FBW (%)	Gain dB
[5]	1.61–1.84, 2.08–2.5	50 × 50	$0.29\lambda \times 0.29\lambda \times 0.01\lambda$	13.4, 19.4	1.8@ 1.72, 1.6@ 2.17 GHz
[8]	0.824–0.96, 1.71–2.26	122 × 60	$0.34\lambda \times 0.16\lambda \times 0.016\lambda$	15.25, 27.7	0.06@ 0.9 GHz, 2.2@ 2 GHz
Proposed	1.6–1.97, 2.34–2.72, 3.89–5.37	48 × 48	$0.26\lambda \times 0.26\lambda \times 0.0084\lambda$	20.72, 15.02, 31.2	1.64@ 1.9 GHz, 2.07@ 2.45 GHz, and 4.06@ 5 GHz

$$\varepsilon_r = \frac{2}{jk_0 d} * \frac{1 - V_1}{1 + V_1} \tag{1}$$

$$\mu_r = \frac{2}{jk_0 d} * \frac{1 - V_2}{1 + V_2} \tag{2}$$

$$n_r = \sqrt{\varepsilon_r \mu_r} \tag{3}$$

where, $V_1 = S_{21} + S_{11}$, $V_2 = S_{21} - S_{11}$, $k_0 = \omega/c$, angular frequency (ω), Slab thickness (d), and light speed (c).

4. ANTENNA PERFORMANCES

The proposed antenna has been designed and simulated using commercially available electromagnetic simulation software CST and HFSS. The designed antenna has been fabricated for experimental validation, shown in Figure 4. The reflection coefficient of the proposed antenna is presented in Figure 5. It is shown from Figure 5 that the proposed antenna has achieved −10 dB measured impedance bandwidth of 370 MHz (1.6–1.97), 380 MHz (2.34–2.72), and 1.48 GHz (3.89–5.37). The simulation results and measured reflection coefficient are seeming identical. Although, a little deviation is observed due to fabrication tolerance.

The Farfield performances of the proposed antenna have been investigated using Satimo near field measurement system, which is presented in Figure 6. The 3D radiation pattern of the proposed antenna has been analyzed at 1.8, 1.9, 2.45, and 5.1 GHz, shown in Figure 7. Moreover, the antenna efficiency and gain have been explored. The radiation efficiency and gain are presented in Figure 8. Figure 8 shows that the measured gain of the proposed antenna at 1.9 GHz is 1.64 dB, 2.45 GHz is 2.07 dB, and 5 GHz is 4.06 dB with radiation efficiency of 66.2%, 77.15%, and 87.6%, respectively. According to the above results, it is shown that the antenna shows better antenna performances than antenna reported in [5] and [8]. A comparison list is presented in Table 2.

5. CONCLUSION

The proposed antenna has been developed for DCS 1800, PCS 1900, WCDMA, Bluetooth, WiMAX, and both lower and upper WLAN applications with good antenna performances in terms of gain, operating bandwidth, radiation efficiency, and radiation patterns. The experimental results matched quite well to the simulated results and demonstrate that the proposed antenna is fully capable to satisfy the mobile applications requirements. The perceptible novelties revealed in this proposed antenna are integrating double negative index metamaterial structure to enhance antenna performances along with size miniaturization.

REFERENCES

1. C.H. Wu and K.L. Wong, Hexa-band internal printed slot antenna for mobile phone application, Microwave Opt Technol Lett 50 (2008), 35–38.
2. T. Alam, M. Faruque, M. Islam, and B. Malaysia, Printed circular patch wideband antenna for wireless communication, Informacije Midem-J Microelectron Electron Compon Mater 44 (2014), 212–217.
3. C. Mahatthanajatuphat, S. Saleekaw, P. Akkaraekthalin, and M. Krairiksh, A rhombic patch monopole antenna with modified minkowski fractal geometry for umts, wlan, and mobile wimax application, Prog Electromagn Res 89 (2009), 57–74.
4. R.B. Waterhouse, Printed antennas for wireless communications, Wiley Online Library, Hoboken, NJ, 2007.
5. S.K. Sharma and R.K. Chaudhary, Dual-band metamaterial-inspired antenna for mobile applications, Microwave Opt Technol Lett 57 (2015), 1444–1447.
6. T. Alam, M.R.I. Faruque, and M.T. Islam, Specific absorption rate reduction of multi-standard mobile antenna with double-negative metamaterial, Electron Lett 51 (2015), 970–971.
7. J.K. Ji, G.H. Kim, and W.M. Seong, A compact multiband antenna based on dng zor for wireless mobile system, IEEE Antennas Wireless Propag Lett 8 (2009), 920–923.
8. L. Li, Z. Jia, F. Huo, and W. Han, A novel compact multiband antenna employing dual-band crlh-tl for smart mobile phone application, IEEE Antennas Wireless Propag Lett 12 (2013), 1688–1691.

FIBER RING RESONATOR USING A CAVITY RING-DOWN INTERROGATION TECHNIQUE FOR CURVATURE SENSING

R. Magalhães, S. O. Silva, and O. Frazão
Faculty of Science, INESC TEC and Department of Physics and Astronomy, University of Porto, Rua Do Campo Alegre, 687, Porto 4169-007, Portugal; Corresponding author: sfsilva@inescporto.pt

ABSTRACT: *In this work, it is demonstrated a fiber ring resonator connected to an interrogation system usually implemented on a cavity ring-down technique. A long-period grating (LPG) was inserted in the resonant cavity, being operated as a curvature sensor. The experimental results demonstrate that using this setup, different sensitivities can be achieved in terms of analyzing decay time over the radius of the curvature and over curvature. The LPG sensor presented higher sensitivity with larger radius of curvature, namely 6.91 μs/m. © 2016 Wiley Periodicals, Inc. Microwave Opt Technol Lett 58:267–270, 2016; View this article online at wileyonlinelibrary.com. DOI 10.1002/mop.29547*

1. INTRODUCTION

Optical couplers are passive devices that couple light through waveguides or fibers. The first singlemode fiber couplers were produced as fused biconical-taper structures, exhibiting low loss, arbitrary branching ratio, polarization independence, and broadband operation in wavelength [1]. These structures are used in many applications including the interface between devices in a system or can be important devices themselves. More advanced
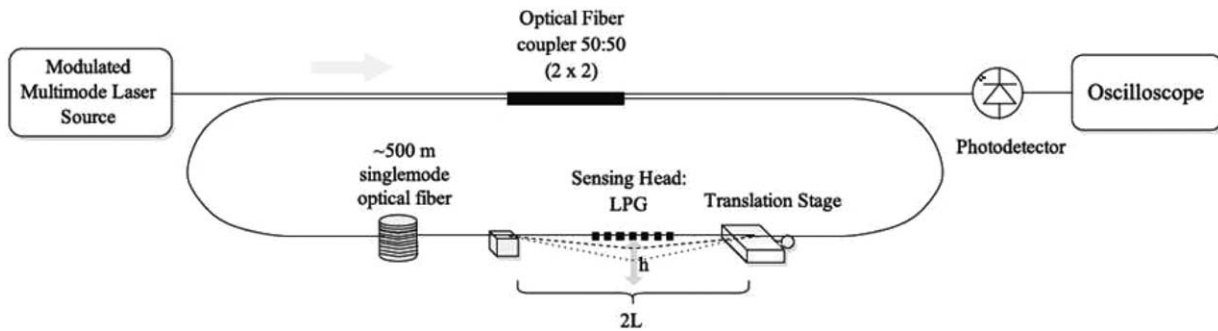
Figure 1 Curvature sensor measuring setup—the signal is introduced by the modulated multimode laser source and monitored by means of a photodetector and an oscilloscope

applications include devices such as polarization converters, mode converters, guided-wave beam splitters, beam combiners, directional couplers, wavelength filters, wavelength multiplexers, and others. Some optical structures, like fiber-ring resonators, integrate optical coupler acting, essentially operating as a power splitter. The first all-fiber-ring resonator was developed in 1982, which used a single strand of singlemode fiber and a directional coupler [2]. Unlike the recent fiber-ring resonator setups, this resonator, although simple, used an active configuration integrating a very complex reading system. Predominantly, fiber-ring resonators can be described as an arrangement of mirrors that form a standing wave cavity resonator for light waves.

Fiber loop reflectors based on fiber couplers were implemented as mirrors in 1988, showing that the reflectivity of the loop strongly depended on the coupling characteristics of the coupler [3]. In 1997, a temperature sensor based on a fiber loop mirror was demonstrated [4]. Recently, these devices are strongly used in optical fiber communications as optical sensors [5].

A more complex structure evolves the combination of optical fibers, a fiber loop and optical couplers, being that technique called Cavity ring-down (CRD) spectroscopy. This approach was developed in 1995, and measures an amplitude modulation with a slow scan, as the cavity decays [6]. This technique has increased popularity as the results with pulsed light sources showed highly sensitive direct absorption results.

This work presents a fiber ring resonator interrogated by a system, usually implemented on the CRD technique. This configuration was developed to measure curvature, being then inserted a long-period grating (LPG) in the resonant cavity, operating as a curvature sensing device. The LPG was used as an intensity sensor when submitted to curvature.

2. EXPERIMENTAL RESULTS

The experimental setup of the proposed system is presented in Figure 1. The main setup is composed by a modulated multimode laser source at 1550 nm, used as a light source to send impulses (5 μs) down into an optical fiber (SMF); a fiber loop ~500 m long jointed with a 3-dB singlemode fiber coupler (2 × 2) to split the signal; and an interrogation system formed by a photodetector with 60 dB internal gain connected to an oscilloscope. An LPG with a central wavelength resonance at 1559 nm, −4.70 dB loss, and a period of 540 μm was also used. The LPG was inserted into the setup, more precisely inside the fiber ring, being than connected to an optical fiber translation stage. This setup formed the proposed curvature sensor measuring system.

The train of pulses travels from the modulated multimode laser source being coupled via 50% arm of the input port; circulates around the fiber loop, being then coupled out via 50% arm of the output port. This system causes an amplitude decay of 50% with time of the output pulses and some other attenuation due to the total existing losses in the fiber loop such as fiber couplers insertion losses, fiber loss, and LPG transmission attenuation. The output signal is guided to the interrogation system where it is detected by the photodetector and read in the oscilloscope. To apply curvature, the LPG was placed inside the
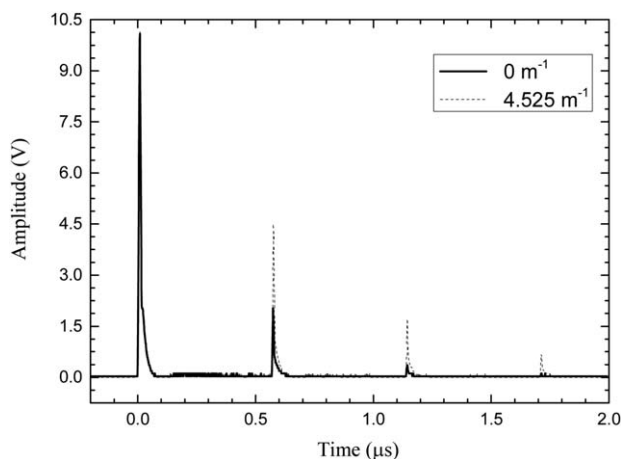
Figure 2 Peak amplitude decay, read in the oscilloscope, versus fiber ring time for zero and maximum curvature applied
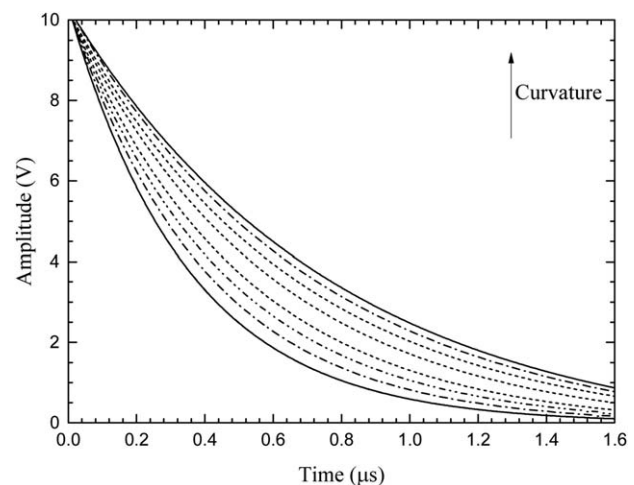
Figure 3 Exponential fitting curves of the decaying pulses for different curvatures applied
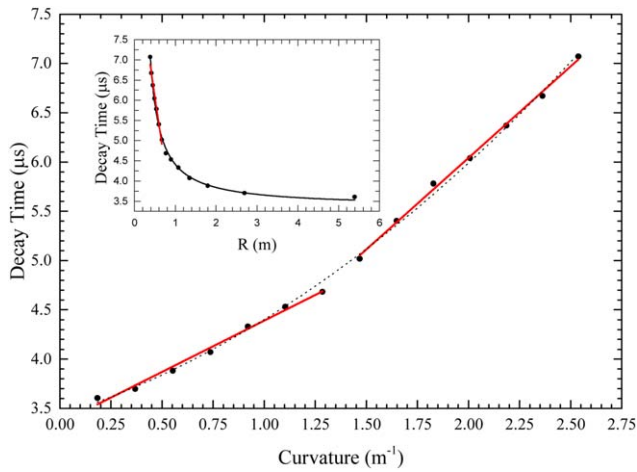
Figure 4 Fiber ring decay time versus applied curvature. Inset, fiber ring decay-time versus the radius of curvature. [Color figure can be viewed in the online issue, which is available at wileyonlinelibrary.com]

fiber ring and fixed at two points that were 104 mm apart, experimenting then sequential curvature by means of a translation stage (via sequential 1 mm displacements). When the LPG is submitted to curvature, it undergoes wavelength and intensity variations. However, in this case, the LPG is used only as an intensity sensor.

The comparison between the amplitude of the peaks obtained with no curvature applied and the maximum curvature applied to the system, respectively, 0 and 4.525 m^{-1}, is shown in Figure 2. The obtained output signal corresponds to the waveform directly observed from the oscilloscope, and shows the amplitude decay of the peaks with time. Using this configuration, the power of peaks is strongly dependent on the ring length. Nonetheless, as the system performs an amplitude decay of consecutive 50%, using a much larger ring, the amount of peaks detected would be categorically identical due to this fast and strong decay.

With no initial curvature applied, the photodetector detected the amplitude decay of the output pulses, and the measured signal was observed in an oscilloscope. When applying the curvature on the LPG, the interrogation system detected a directly proportional relation between the curvature and the amplitude of the output pulses, being so verified the rise of the peaks with increasing curvature. See Figures 2 and 3. Results show that the amplitude of the first peak remains unchanged during the process of curvature application. This happens as the first pulse is coupled out via 50% arm of the output port without circulating around the fiber loop, being so directly interrogated by the photodiode. Successive pulses are a result of consecutive trips in the resonator, which outcomes as amplitude decay of 50% with time.

The analysis reproduced for several curvature displacement values is illustrated in Figure 3. Initially, the peaks obtained for

a great part of the displacements were isolated and an exponential fit was performed. These values depend on the attenuation of the fiber, the losses originated by the length of the loop, splices, and insertion loss of the fiber coupler.

The behavior of the decay time was characterized as a function of curvature ($1/R$) and outlined in Figure 4. The change in the curvature was measured according to $2h/(h^2 + L^2)$ [7], where L is the half distance between the two fixed points. The amplitude of the signal increases with increasing curvature, as result of bending the LPG. The characterization of the decay time as a function of R (radius of curvature) is shown in inset of Figure 4. The sensitivities for curvature and R were also analyzed and compared, as presented in Figure 4.

Table 1 shows the different sensitivities obtained, corresponding to the respective intervals of time. For the interval [5.01, 7.07] μs, the sensitivities obtained were 6.91 $\mu s/m$ and 1.86 $\mu s/m^{-1}$, using the radius of curvature and curvature, respectively. Being the sensitivity $\sim 6 \times$ greater using R when comparing to curvature, one can indicate the preferential use of R instead of curvature, in this temporal spectrum. For the interval [3.69, 4.67] μs, it was registered a sensitivity of 1.04 $\mu s/m^{-1}$ using the curvature, and no sensitivity was observed using R instead, as it is shown in Figure 4. Therefore, analyzing the decay time over curvature, a linear response was obtained (differing from what happens using the radius), which indicates the necessary use of this parameter to obtain such behavior. To analyze these results, two linear fits were performed, adding up a third polynomial fit performed to all data.

3. CONCLUSION

Summarizing, it was presented a fiber ring resonator interrogated by a CRD-based technique. This configuration used an LPG that worked as an intensity sensor when submitted to curvature.

Curvature was applied to the LPG in the range of 0–4.52 m^{-1}. It was demonstrated the rise of the amplitude peaks with increasing curvature in this interval, being so verified the sensitive behavior of the grating when subjected to external deflection. The first peak remained unchanged during the curvature application process, as the first pulse travels directly to the photodiode through the output port, without circulating in the loop.

Experimental results indicated that the sensing structure registered highest sensitivity using R rather than the curvature. This last one presented sensitivities of 1.04 $\mu s/m^{-1}$ and 1.86 $\mu s/m^{-1}$ in the time periods [3.69, 4.67] μs and [5.01, 7.07] μs, respectively. Conversely, although the nonlinear results obtained, using the radius of the curvature one can obtain a sensitivity of 6.91 $\mu s/m$ in the interval [5.01, 7.07] μs—this corresponds to a much better sensitivity, approximately $6 \times$ higher compared with the curvature.

TABLE 1 Sensitivities to Curvature and R in Different Decay Time Ranges

Decay Time Interval μs	Curvature $\mu s/m^{-1}$	Radius of Curvature (R) $\mu s/m$
[3.69, 4.67]	1.04	Insensitive
[5.01, 7.07]	1.86	6.91

REFERENCES

1. B.S. Kawasaki, K.O. Hill, and R.G. Lamont, Biconical-taper single-mode fiber coupler, Opt Lett 6 (1981), 327–328.

2. L.F. Stokes, M. Chodorow, and H.J. Shaw, All-single-mode fiber resonator, Opt Lett 7 (1982), 288–290.

3. P. Hariharan, Optical interferometry, 2nd ed., Academic, New York, 2003.

4. A. Küng, J. Budin, L. Thévenaz, and Ph. A. Robert, Optical fibre ring resonator characterization by optical time-domain reflectometry, Opt Lett 22 (1997), 90–92.

5. J. Capmany and M.A. Muriel, Double-cavity fibre structures as all optical timing extraction circuits for gigabit networks, Fibre Integr Opt 12 (1993), 247–255.

6. A. Melloni, Synthesis of a parallel-coupled ring-resonator filter, Opt Lett 26 (2001), 917–919.

7. S. Silva, E.G.P. Pachon, M.A.R. Franco, P. Jorge, J.L. Santos, F. Xavier Malcata, C.M.B. Cordeiro, and O. Frazão, Curvature and temperature discrimination using multimode interference fiber optic structures—A proof of concept, J Lightwave Technol 30 (2012), 3569–3575.

A COMPACT FOUR ELEMENTS UWB MIMO ANTENNA WITH ON-DEMAND WLAN REJECTION

Saeed M. Khan,[1] **Adnan Iftikhar,**[2,3] **Sajid M. Asif,**[2,3]
Antonio-Daniele Capobianco,[1] **and Benjamin D. Braaten**[2]
[1] Dipartimento Di Ingegneria Dell'informazione, University of Padova via Gradenigo 6/B, Padova 35131, Italy; Corresponding author: Khan@dei.unipd.it
[2] Department of Electrical and Computer Engineering, North Dakota State University, Fargo, ND 58102
[3] Department of Electrical and Computer Engineering, COMSATS Institute of Information Technology Park Road, Islamabad, Pakistan

ABSTRACT: *This article presents a four elements frequency reconfigurable ultrawideband (UWB) multiple-input-multiple-output (MIMO) design, capable of rejecting on-demand WLAN band ranging from 4.8 to 6.2 GHz. The proposed design consists of two U-shaped monopole UWB radiators and two circular slotted-monopole radiators. These monopole radiators are placed orthogonally with respect to each other to exploit polarization diversity, whereas the PIN diodes are used to connect the band-stop design with the ground plane to introduce the on-demand band rejection feature. An isolation of better than 17 dB between the four UWB-MIMO elements is achieved in the 2.7–12 GHz frequency range for the both PIN diodes biased and unbiased states. The simulations and measurements results showed good agreement over the band of interest.* © 2016 Wiley Periodicals, Inc. Microwave Opt Technol Lett 58:270–276, 2016; View this article online at wileyonlinelibrary.com. DOI 10.1002/mop.29546

1 INTRODUCTION

In high-speed wireless communication technologies such as, wireless personal area networks, ultrawide band (UWB) multiple-input-multiple-output (MIMO) antennas have been considered to be an integral part of the communication system. However, WLAN signals (in the 5.15–5.35 and 5.75–5.8225 GHz bands) may interfere with those of UWB (3.1–10.6 GHz) technology and causing detrimental effects. So, for this reason designers have used different techniques in band-reject UWB or UWB-MIMO antennas [1–9]. In [1], slots have been used in the radiator to get the dual band notched characteristics, while in [2] a pair of slits has been inserted in the radiators to achieve the band-notch functionality. Moreover, related works in [3–5] involve insertion of stubs to reject the WLAN bands and introduction of the polarization diversity to improve the isolation among the elements. An electromagnetic bandgap structure has also been implemented to reject the WLAN band along with the band-stop filter for coupling suppression in [6]. Rejection of WLAN band has been implemented using a short stub and parasitic meander lines were inserted to reduce the mutual coupling in [7]. In [8], different types of resonators were used to attain the band notch functionality and also polarization diversity between nearly placed elements was exploited to attain high isolation. Another technique in [9], involves the insertion of stubs in the ground plane to mitigate the interference between the UWB and WLAN bands. Moreover, a $\lambda/2$ length of open stub has also been used on the ground plane $(55 \times 86.5$ mm$^2)$ of the antenna having a large reflector size [7]. Generally, previous works dealing with the band rejection either emphasized on rejecting the multiple bands or a portion of the band only permanently. Also, most of the designs in the literature focus on the band rejection feature of two elements UWB MIMO antennas.

In this article, a four elements frequency reconfigurable UWB MIMO antenna shown in Figure 1 is proposed for the on-demand band rejection. Two UWB monopole radiators in the proposed structure have rectangular slot whereas the others have circular slots. The ground plane of all the four radiators is shared using a rectangular shortening strip, as shown in Figure 1(b). In the proposed design, high isolation between the elements was achieved by exploiting the polarization diversity between nearly placed elements. The on-demand band rejection is achieved using the PIN diodes which connect the shared ground plane with the band-stop design. The detailed description of the design, and simulated and measured results will be discussed in the following sections.

2 FOUR ELEMENTS UWB MIMO ANTENNA DESIGN

2.1. Antenna Geometry and Biasing Circuit

The detailed geometry of the proposed design is shown in Figure 1. Two U-shaped slot monopole radiators and two circular slot monopole radiators with tapered section feeding are shown in Figure 1. One U-shaped slot radiator was placed orthogonally to the circular slot radiator at a distance of 1 mm. Similarly, the second U-shaped slot radiator was placed perpendicular to the other circular slot radiator at a same distance. These slots had been used to improve the broadband matching. The placement is chosen in such a way that there exists broadband matching characteristic, polarization diversity, and high isolation. Later on, the ground planes of all these radiators were connected through a shortening strip of $c_g=0.5$ mm width. A small change in the return loss and isolation was observed. But the impedance matching in the 2.7–12 GHz frequency range was achieved. A small patch of size $l_{g3} \times w_{g3}$ was also connected with the ground plane so that a symmetrical design of band-stop design could be attached to the ground plane to reject the WLAN band. Next, on the bottom side of the proposed structure a band-stop design is inserted and the length of the band-stop design is determined using the formula $L_{b_1} = \frac{\lambda}{2} = \left(\frac{c}{(f_0 \times \sqrt{\epsilon_r})}\right)$ where $f_0 = 5.5$ GHz is the central frequency of the rejected band and ϵ_r is the relative permittivity of the substrate. The stubs in the band-stop design act as an inductor whereas, gaps between the stubs